

Doping-Dependent and Orbital-Dependent Band Renormalization in $\text{Ba}(\text{Fe}_{1-x}\text{Co}_x)_2\text{As}_2$ Superconductors

T. Sudayama,¹ Y. Wakisaka,¹ T. Mizokawa,^{2,1} S. Ibuka,^{3,4} R. Morinaga,^{3,4}
T. J. Sato,^{3,4} M. Arita,⁵ H. Namatame,⁵ M. Taniguchi,^{5,6} and N. L. Saini^{7,2}

¹*Department of Physics, University of Tokyo, 5-1-5 Kashiwanoha, Kashiwa, Chiba 277-8561, Japan*

²*Department of Complexity Science and Engineering, University of Tokyo,*

5-1-5 Kashiwanoha, Kashiwa, Chiba 277-8561, Japan

³*Institute for Solid State Physics, University of Tokyo, 106-1 Shirakata, Tokai, Ibaraki 319-1106, Japan*

⁴*JST, TRIP, 5, Sanbancho, Chiyoda, Tokyo 102-0075, Japan*

⁵*Hiroshima Synchrotron Radiation Center, Hiroshima University, Higashihiroshima, Hiroshima 739-0046, Japan*

⁶*Graduate School of Science, Hiroshima University, Higashihiroshima, Hiroshima 739-8526, Japan*

⁷*Department of Physics, Università di Roma "La Sapienza", Piazzale Aldo Moro 2, 00185 Roma, Italy*

(Dated: March 8, 2013)

Angle resolved photoemission spectroscopy of $\text{Ba}(\text{Fe}_{1-x}\text{Co}_x)_2\text{As}_2$ ($x = 0.06, 0.14$, and 0.24) shows that the width of the Fe $3d$ yz/zx hole band depends on the doping level. In contrast, the Fe $3d$ $x^2 - y^2$ and $3z^2 - r^2$ bands are rigid and shifted by the Co doping. The Fe $3d$ yz/zx hole band is flattened at the optimal doping level $x = 0.06$, indicating that the band renormalization of the Fe $3d$ yz/zx band correlates with the enhancement of the superconducting transition temperature. The orbital-dependent and doping-dependent band renormalization indicates that the fluctuations responsible for the superconductivity is deeply related to the Fe $3d$ orbital degeneracy.

PACS numbers:

I. INTRODUCTION

Research activities to understand fundamental mechanisms of high temperature superconductivity have been accelerated by the discovery of superconductivity in the FeAs systems^{1,2}. The FeAs-based superconductors commonly have the FeAs layers where Fe atoms are tetrahedrally coordinated by As, and are obtained by carrier doping to the antiferromagnetic parent compounds such as LaFeAsO and BaFe_2As_2 . BaFe_2As_2 shows superconductivity by electron doping with the highest T_c of 25 K in $\text{Ba}(\text{Fe},\text{Co})_2\text{As}_2$ although the FeAs plane is highly disordered by the Co doping^{3,4}. Since the superconducting phase is closely related to the magnetic phase in the FeAs-based as well as CuO-based high- T_c superconductors, many experimental and theoretical studies have been dedicated to understand the relationship between the superconductivity and magnetism⁵. When the $3d$ electrons are localized to form a Mott insulator, the symmetry of transition-metal $3d$ orbitals controls the magnetic interaction between the transition-metal $3d$ spins (Kugel-Khomskii mechanism), while the symmetry breaking of the transition-metal $3d$ orbitals is accompanied by the local lattice distortion (Jahn-Teller mechanism)⁶. When the $3d$ electrons are itinerant, the band Jahn-Teller effect coupled with lattice distortion can change the Fermi surface topology to induce magnetic instability (Orbitally-induced Peierls mechanism)⁷. Actually, the anomalous lattice instability is commonly found in the various high- T_c superconductors including the cuprate-based and Fe-based superconductors^{8,9}. In this context, the transition-metal $3d$ orbital degree of freedom is the key ingredient which bridges between the lattice instability and the magnetic instability both in

localized and itinerant cases.

The angle-resolved photoemission spectroscopy (ARPES) is a powerful technique to study the electronic structure of multi-orbital systems where the lattice and magnetic instabilities may exist. As for the FeAs systems, ARPES studies on hole-doped¹⁰⁻¹³ and electron-doped¹⁴⁻²⁰ BaFe_2As_2 have confirmed the importance of the multi-orbital character as predicted by the band-structure calculations^{19,21,22}. However, the effect of Co doping on evolution of multi-orbital electronic structure is rather complicated²³ and should be examined further to understand the fundamental mechanism of the superconductivity. Here, we report an ARPES study on $\text{Ba}(\text{Fe}_{1-x}\text{Co}_x)_2\text{As}_2$ with $x = 0.06, 0.14$, and 0.24 around Γ point. It has been found that the upward chemical potential shift with the Co doping basically supports the electron doping picture. However, while the renormalization factor for the $3z^2 - r^2$ and $x^2 - y^2$ bands does not depend on the doping level, that for the yz/zx hole band decreases with the Co doping breaking the simple rigid band model. The band narrowing of the yz/zx hole band correlates with the enhancement of T_c , indicating that the orbital effect plays important roles for the mechanism of high- T_c superconductivity.

Single crystals of $\text{Ba}(\text{Fe}_{1-x}\text{Co}_x)_2\text{As}_2$ with $x = 0.06, 0.14$, and 0.24 were grown by Bridgman method with FeAs flux²⁴. ARPES measurements were performed at beam line 9A, Hiroshima Synchrotron Radiation Center (HSRC) using a SCIENTA R4000 analyzer with circularly polarized light ($h\nu = 17$ eV and 23 eV). Total energy resolutions were set to 18 meV and 14 meV for $h\nu = 23$ eV and 17 eV, respectively. We cleaved the single crystals at 30 K under ultrahigh vacuum of 5×10^{-9} Pa

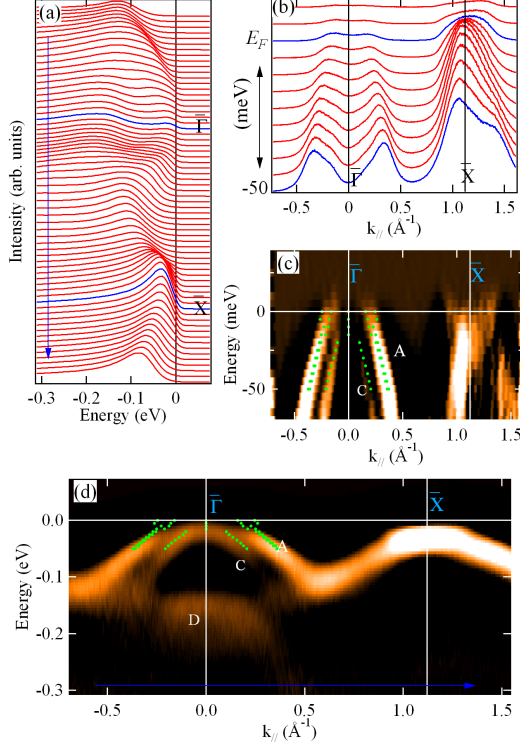


FIG. 1: (Color online) (a) EDC plot and (b) MDC plot for $x=0.06$ taken at $h\nu = 23$ eV. (c) Second derivative plot of MDC. (d) Second derivative plot of EDC. The dots indicate the band locations determined by fitting MDCs to Lorentzian functions. The $\bar{\Gamma}$ - \bar{X} direction is the nearest neighbor Fe-Fe direction in the plane.

and the ARPES data of the cleaved surface parallel to the FeAs plane were collected at 30 K within four hours after the cleaving.

Figures 1(a) and (b) show energy distribution curve (EDC) and momentum distribution curve (MDC) plots of the ARPES data for $x=0.06$ (optimally-doped system) taken at $h\nu = 23$ eV from the zone center ($\bar{\Gamma}$ point) to the zone corner (\bar{X} point) of the two-dimensional Brillouin zone. The in-plane momentum $k_{||}$ is swept along the nearest neighbor Fe-Fe direction in the plane. At $h\nu = 23$ eV, the $\bar{\Gamma}$ point corresponds to the Γ point of the three-dimensional Brillouin zone where the out-of plane momentum k_z is zero. The second derivative plots of MDC and EDC are displayed in Figs. 1(c) and (d), respectively. By comparing the present result with the band structure calculation near the Γ point¹⁹, the parabolic band crossing E_F can be assigned to one of the yz/zx bands (band A). Here, the z axis is perpendicular to the FeAs plane and the x axis is along the nearest neighbor Fe-Fe direction in the plane. On the other hand, the other hole band takes its maximum at ~ -10 meV and can be assigned to the $x^2 - y^2$ band (band C). The broad and flat band at ~ -170 meV is identi-

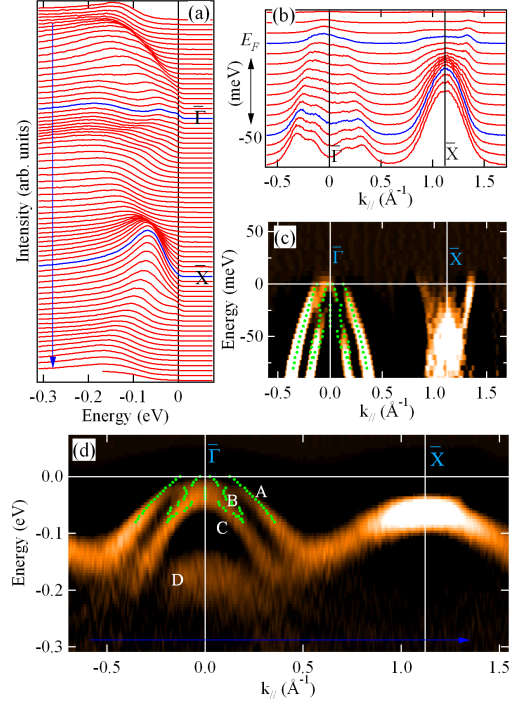


FIG. 2: (Color online) (a) EDC plot and (b) MDC plot for $x=0.14$ taken at $h\nu = 23$ eV. (c) Second derivative plot of MDC. (d) Second derivative plot of EDC. The dots indicate the band locations determined by fitting MDCs to Lorentzian functions. The $\bar{\Gamma}$ - \bar{X} direction is the nearest neighbor Fe-Fe direction in the plane.

fied as the $3z^2 - r^2$ band (band D). The observation of the two hole bands (bands A and C) in the optimally-doped system is apparently inconsistent with that of the three hole bands in the overdoped system (bands A, B and C, see Fig. 2)¹⁸. In order to further examine this apparent inconsistency, we have tried to determine the band locations of the two hole bands by fitting MDCs to Lorentzian functions. The results are shown by the dots in Figs. 1 (c) and (d). Interestingly, the yz/zx hole band (band A) near E_F (in the region above -10 meV) is found to become broad in the momentum space compared to that below -10 meV. Consequently, it is possible to fit the broad yz/zx hole band to the two components in the energy region from E_F to -10 meV although the fitting to the two components is just to demonstrate the broadening and is not a unique solution. Below -10 meV, the two components merge to form the single yz/zx hole band, indicating that band A becomes narrow below -10 meV compared to that above -10 meV. The disappearance of band B can be attributed to the smearing effect of k_z dispersion and/or the photoemission matrix element effect¹¹. However, in the ARPES measurements under various conditions¹⁴⁻²⁰, band B is always absent near the

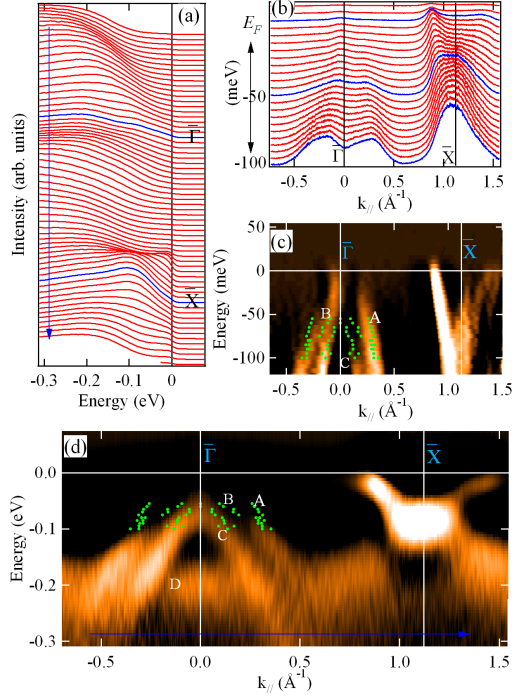


FIG. 3: (Color online) (a) EDC plot and (b) MDC plot for $x=0.24$ taken at $\hbar\nu = 23$ eV. (c) Second derivative plot of MDC. (d) Second derivative plot of EDC. The dots indicate the band locations determined by fitting MDCs to Lorentzian functions. The $\bar{\Gamma}$ - \bar{X} direction is the nearest neighbor Fe-Fe direction in the plane.

Γ point, suggesting that the absence of band B is not due to the smearing effect of k_z dispersion and/or the matrix element effect.

EDC and MDC plots for $x = 0.14$ (overdoped system) taken at $\hbar\nu = 23$ eV are displayed in Figs. 2(a) and (b), respectively. Figures 2(c) and (d) shows the second derivative plots made up from the MDC and EDC data, respectively. Three parabolic bands can be identified around the zone center and two of them (bands A and B) reach E_F . In this plot, the three hole bands are identified by fitting MDCs to Lorentzian functions as already reported in the literature¹⁸. By comparing the EDC data in Fig. 2(a) to that in Fig. 1(a), the hole bands at the zone center are sharpened and the electron bands at the zone corner are broadened in going from the optimally-doped system to the overdoped system.

Figures 3(a) and (b) show EDC and MDC plots for $x = 0.24$ (heavily-overdoped system) taken at $\hbar\nu = 23$ eV, respectively. In the heavily-overdoped system, the hole bands at the zone center are very broad in the EDC plot probably because the hole bands are fully occupied by electrons and are located well below E_F . Assuming that three hole bands should exist, the broad

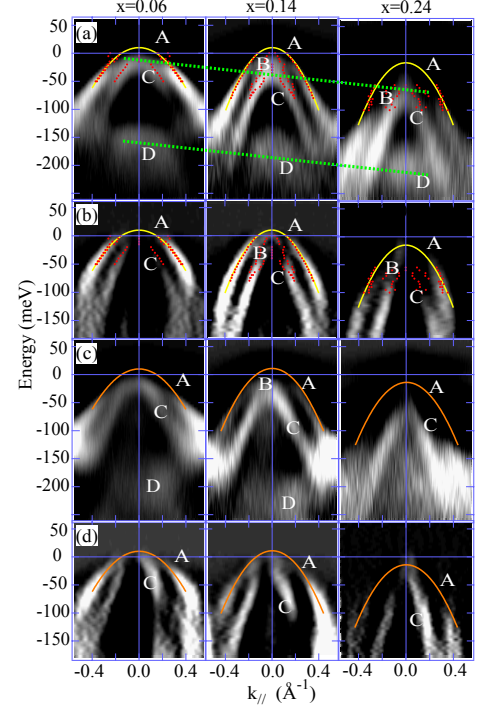


FIG. 4: (Color online) (a) Second derivative plots for $x=0.06$, 0.14 , and 0.24 at $\hbar\nu = 23$ eV. The dots indicate the band locations determined by fitting the MDCs to Lorentzian functions. The solid parabolic curves roughly show the dispersion of hole band A. The dotted lines roughly show the energy shift of top of hole band C and that of band D. (b) Second derivative plots of MDC for $x=0.06$, 0.14 , and 0.24 at $\hbar\nu = 23$ eV. (c) Second derivative plots of EDC for $x=0.06$, 0.14 , and 0.24 at $\hbar\nu = 17$ eV. (d) Second derivative plots of MDC for $x=0.06$, 0.14 , and 0.24 at $\hbar\nu = 17$ eV.

MDC data can be fitted to the model Lorentzian functions with three components. In the second derivative plots displayed in Figs. 3(c) and (d), the band locations of the three components determined by the fitting are plotted. In the heavily-overdoped case, the hole bands never reach E_F , consistent with the electron doping from $x=0.14$ to $x=0.24$ and the result of neutron scattering experiment²⁵.

The second derivative plot of MDC is useful to identify the dispersive bands while the dispersionless band can be found in the second derivative plot of EDC. In Figs. 4 (a) and (b), the second derivative plots of EDC and MCD for the hole bands around the Γ point are displayed in order to show the evolution of the hole band dispersions as a function of the Co doping. Firstly, the top of hole band C (the $x^2 - y^2$ band) is located at -10 meV, -30 meV, and -50 meV for $x = 0.06$, 0.14 , and 0.24 , respectively. This energy shift [indicated by the dotted

line in Fig. 4(a)] is consistent with the upward chemical potential shift by the electron doping. The flat band at ~ -170 meV (band D) can be assigned to the renormalized $3z^2 - r^2$ band which is located at ~ -700 meV in the LDA calculation²¹. Band D also shows the same energy shift as band C. The discrepancy between the experimental results and the band-structure calculations can be explained by the band renormalization due to correlation effects. Figure 4 shows that the degree of the band renormalizations for the $x^2 - y^2$ and $3z^2 - r^2$ bands does not depend on the doping level. These two bands show rigid band energy shift due to the chemical potential shift by the Co doping. Secondly, the slope of hole band A (one of the yz/zx bands) increases from the optimally doped system to the overdoped system. In Fig. 4, the dispersion of hole band A is roughly shown by the solid parabolic curves which are given by $E = ak^2 + b$. Here, E and k are energy (in unit of eV) and momentum (in unit of \AA^{-1}) of the electron, respectively. In the optimally doped system, $a = -0.45$ and $b = 0.01$, while $a = -0.70$ (-0.70) and $b = 0.01$ (-0.015) for the overdoped (heavily-overdoped) system. In the region of $0.25\text{\AA}^{-1} < k_{\parallel} < 0.35\text{\AA}^{-1}$, the energy difference between the highest and the lowest energy states are about 25 meV and 40 meV for $x=0.06$ and $x=0.14$, respectively. Considering the accuracy of energy (less than 1 meV) and k_{\parallel} (less than 0.01\AA^{-1}), one can safely conclude that the width of hole band A is considerably reduced in the optimally doped system. Figures 4 (c) and (d) show the second derivative plots of EDC and MCD taken at $h\nu = 17$ eV for the hole bands at the zone center. At $h\nu = 17$ eV, the $\bar{\Gamma}$ point corresponds to the midpoint of Γ and Z points of the three-dimensional Brillouin zone. The hole bands observed at $h\nu = 17$ eV are slightly flattened compared to those at $h\nu = 23$ eV due to the difference of the out-of plane momentum k_z . The dispersions of hole band A are roughly given by $a = -0.45$ and $b = 0.01$, $a = -0.58$ and $b = 0.01$, and $a = -0.58$ and $b = -0.015$ for the optimally doped, overdoped, and heavily-overdoped systems. Although the width of hole band A decreases from Γ to Z in the

overdoped system, it is further reduced in going from the overdoped system to the optimally doped system.

The above ARPES results show that the yz/zx hole bands are strongly modified at the optimal doping level. The band deformation would be related to the recent theoretical and experimental works on the essential role of orbital degrees of freedom in the Fe-based superconductors^{26,27}. The tetragonal-to-orthorhombic structural transition temperature is extrapolated to 0 K at the optimal doping. Therefore, one can speculate that the doping dependence of the orbital-selective band renormalization is related to the orthorhombic lattice fluctuation, which can couple with the yz/zx orbitals and can provide inhomogeneity of orbital and lattice. Further theoretical and experimental studies are required to understand whether the orbital or lattice fluctuation really contributes to the pairing mechanism or not. However, at least, this type of orbital or lattice fluctuation is expected to enhance the spin fluctuation via the orbitally-induced Peierls coupling⁷ or the orbitally-induced excitonic coupling²⁸.

In conclusion, the angle resolved photoemission spectroscopy study on $\text{Ba}(\text{Fe}_{1-x}\text{Co}_x)_2\text{As}_2$ ($x = 0.06, 0.14$, and 0.24) reveals the orbital- and doping-dependent band renormalization. In the optimally-doped system, the renormalization factor of the observed yz/zx hole band is strongly enhanced compared to that in the overdoped regimes. In contrast, the $x^2 - y^2$ and $3z^2 - r^2$ bands show rigid band energy shift due to the Co doping and their renormalization factors do not depend on the doping level. The orbital- and doping-dependent band renormalization indicates that the orbital degree of freedom of the yz/zx hole bands may play an essential role to enhance superconducting transition temperature.

This work was supported in part by the Global COE Program "the Physical Sciences Frontier", MEXT, Japan. The synchrotron radiation experiments have been done with the approval of HSRC (Proposals No. 09-A-25 and No. 10-A-10)

- ¹ Y. Kamihara, T. Watanabe, M. Hirano, and H. Hosono: J. Am. Chem. Soc. **130** (2008) 3296.
- ² H. Takahashi, K. Igawa, K. Arii, Y. Kamihara, M. Hirano, and H. Hosono: Nature **453** (2008) 376.
- ³ A. S. Sefat, R. Jin, M. A. McGuire, B. C. Sales, D. J. Singh, and D. Mandrus: Phys. Rev. Lett. **101** (2008) 117004.
- ⁴ Y. Nakajima, T. Taen, and T. Tamegai: J. Phys. Soc. Jpn. **78** (2009) 023702.
- ⁵ P. A. Lee, N. Nagaosa, and X.-G. Wen: Rev. Mod. Phys. **78** (2006) 17.
- ⁶ K. Kugel and D. I. Khomskii: Zh. Eksp. Teor. Fiz. **15** (1973) 1429 [Sov. Phys. JETP. **37** (1973) 725].
- ⁷ D. I. Khomskii and T. Mizokawa: Phys. Rev. Lett. **94** (2005) 156402.
- ⁸ N. L. Saini, H. Oyanagi, and A. Bianconi: J. Phys. Soc. Jpn. **70** (2001) 2092.

- ⁹ B. Joseph, A. Iadecola, A. Puri, L. Simonelli, Y. Mizuguchi, Y. Takano, and N. L. Saini: Phys. Rev. B **82** (2010) 020502.
- ¹⁰ H. Ding, P. Richard, K. Nakayama, K. Sugawara, T. Arakane, Y. Sekiba, A. Takayama, S. Souma, T. Sato, T. Takahashi, Z. Wang, X. Dai, Z. Fang, G. F. Chen, J. L. Luo, and N. L. Wang: Europhys. Lett. **83** (2008) 47001.
- ¹¹ C. Liu, G. D. Samolyuk, Y. Lee, N. Ni, T. Kondo, A. F. Santander-Syro, S. L. Bud'ko, J. L. McChesney, E. Rotenberg, T. Valla, A. V. Fedorov, P. C. Canfield, B. N. Harmon, and A. Kaminski: Phys. Rev. Lett. **101** (2008) 177005.
- ¹² V. B. Zabolotnyy, D. S. Inosov, D. V. Evtushinsky, A. Koitzsch, A. A. Kordyuk, G. L. Sun, J. T. Park, D. Haug, V. Hinkov, A. V. Boris, C. T. Lin, M. Knupfer, A. N. Yaresko, B. Büchner, A. Varykhalov, R. Follath, and S. V.

- Borisenko: *Nature* **457** (2009) 569.
- ¹³ Y. Zhang, J. Wei, H. W. Ou, J. F. Zhao, B. Zhou, F. Chen, M. Xu, C. He, G. Wu, H. Chen, M. Arita, K. Shimada, H. Namatame, M. Taniguchi, X. H. Chen, and D. L. Feng: *Phys. Rev. Lett.* **102** (2009) 127003.
 - ¹⁴ K. Terashima, Y. Sekiba, J. H. Bowen, K. Nakayama, T. Kawahara, T. Sato, P. Richard, Y.-M. Xu, L. J. Li, G. H. Cao, Z.-A. Xu, H. Ding, and T. Takahashi: *Proceedings of the National Academy of Sciences of the USA (PNAS)* **106** (2009) 7330.
 - ¹⁵ Y. Sekiba, T. Sato, K. Nakayama, K. Terashima, P. Richard, J. H. Bowen, H. Ding, Y.-M. Xu, L. J. Li, G. H. Cao, Z.-A. Xu and T. Takahashi: *New J. Phys.* **11** (2009) 025020.
 - ¹⁶ P. Vilmercati, A. Fedorov, I. Vobornik, U. Manju, G. Panaccione, A. Goldoni, A. S. Sefat, M. A. McGuire, B. C. Sales, R. Jin, D. Mandrus, D. J. Singh, and N. Mannella: *Phys. Rev. B* **79** (2009) 220503(R).
 - ¹⁷ W. Malaeb, T. Yoshida, A. Furimori, M. Kubota, K. Ono, K. Kihou, P. M. Shirage, H. Kito, A. Iyo, H. Eisaki, Y. Nakajima, T. Tamegai, and R. Arita: *J. Phys. Soc. Jpn.* **78** (2009) 123706.
 - ¹⁸ T. Sudayama, Y. Wakisaka, K. Takubo, R. Morinaga, T. J. Sato, M. Arita, H. Namatame, M. Taniguchi, and T. Mizokawa: *Phys. Rev. Lett.* **104** (2010) 177002.
 - ¹⁹ S. Thirupathaiah, S. de Jong, R. Ovsyannikov, H. A. Dürr, A. Varykhalov, R. Follath, Y. Huang, R. Huisman, M. S. Golden, Yu-Zhong Zhang, H. O. Jeschke, R. Valent[?], A. Erb, A. Gloskovskii, and J. Fink: *Phys. Rev. B* **81** (2010) 104512.
 - ²⁰ B. Mansart, V. Brouet, E. Papalazarou, M. Fuglsang Jensen, L. Petaccia, S. Gorovikov, A. N. Grum-Grzhimailo, F. Rullier-Albenque, A. Forget, D. Colson, and M. Marsi: *Phys. Rev. B* **83** (2011) 064516.
 - ²¹ D. J. Singh: *Phys. Rev. B* **78** (2008) 094511.
 - ²² K. Kuroki, S. Onari, R. Arita, H. Usui, Y. Tanaka, H. Kontani, and H. Aoki: *Phys. Rev. Lett.* **101** (2008) 087004.
 - ²³ H. Wadati, I. Elfimov, and G. A. Sawatzky: *Phys. Rev. Lett.* **105** (2010) 157004.
 - ²⁴ R. Morinaga, K. Matan, H. S. Suzuki, and T. J. Sato: *Jpn. J. Appl. Phys.* **48** (2009) 013004.
 - ²⁵ K. Matan, S. Ibuka, R. Morinaga, Songxue Chi, J. W. Lynn, A. D. Christianson, M. D. Lumsden, and T. J. Sato: *Phys. Rev. B* **82**, 054515 (2010).
 - ²⁶ H. Kontani and S. Onari: *Phys. Rev. Lett.* **104** (2010) 157001.
 - ²⁷ S.-H. Lee, Guangyong Xu, W. Ku, J. S. Wen, C. C. Lee, N. Katayama, Z. J. Xu, S. Ji, Z. W. Lin, G. D. Gu, H.-B. Yang, P. D. Johnson, Z.-H. Pan, T. Valla, M. Fujita, T. J. Sato, S. Chang, K. Yamada, and J. M. Tranquada: *Phys. Rev. B* **81** (2010) 220502(R).
 - ²⁸ T. Mizokawa, T. Sudayama, and Y. Wakisaka: *J. Phys. Soc. Jpn.* **77** Supplement C (2008) 158.